L_1-L_3 Coster-Kronig yield for elements with $70 \leqslant Z \leqslant 81$

Manju Sharma,[1] Prem Singh,[1] Sanjiv Puri,[2] D. Mehta,[1] and Nirmal Singh[1]
[1]*Department of Physics, Panjab University, Chandigarh 160 014, India*
[2]*Department of Physics, SLIET, Longowal 148 106, India*
(Received 22 July 2003; published 11 March 2004)

The L_1-L_3 Coster-Kronig (CK) yield f_{13} for the $_{70}$Yb, $_{71}$Lu, $_{74}$W, $_{75}$Re, $_{79}$Au, $_{80}$Hg, and $_{81}$Tl elements was deduced using measured intensities of the $L\alpha$ x rays emitted following decay of the L_i-subshell ($i=1,2,3$) vacancies produced in widely different proportions by the 59.54 keV γ rays ($B_{L_1} < E_{inc} < B_K$) and the Ge/Se/Rb K x rays ($B_{L_3} < E_{K\alpha} < B_{L_2}, B_{L_1/L_2} < E_{K\beta} < B_K$); where $B_{K/Li}$ is the K-shell/L_i-subshell binding energy of the target element. An energy-dispersive x-ray fluorescence set up, involving photon sources consisting of a ^{241}Am annular source in the direct and secondary excitation modes along with the Ge/Se/RbCl secondary exciter and a Si(Li) detector, was used for the measurements. The measured f_{13} yields for $_{70}$Yb, $_{71}$Lu, and $_{74}$W are found to agree with the values based on the relativistic Dirac-Hartree-Slater (RDHS) calculations, while those for $_{79}$Au, $_{80}$Hg, and $_{81}$Tl are lower by ~20%. The measured f_{13} yields exhibit a jump from 0.354(24) for $_{74}$W to 0.450(27) for $_{75}$Re compared to that from 0.352 to 0.640 as predicted by the RDHS calculations due to onset of the intense L_1-L_3M_5 CK transition.

DOI: 10.1103/PhysRevA.69.032501 PACS number(s): 32.30.Rj, 32.80.Fb, 32.80.Hd, 33.50.−j

I. INTRODUCTION

The L_i-subshell ($i=1,2,3$) vacancy decays either through the x ray, Auger (intershell hole transfer), or Coster-Kronig (intrashell hole transfer) transition. Also, there exists a small probability of radiative L_1-L_3 Coster-Kronig (CK) transition in the heavy elements. The L_i-subshell ($i=1,2,3$) radiative transition probabilities based on the relativistic Hartree-Slater calculations have been tabulated by Scofield [1] for all the elements with $5 \leqslant Z \leqslant 104$. The Auger and CK transition probabilities based on the relativistic Dirac-Hartree-Slater (RDHS) calculations have been tabulated by Chen, Crasemann, and Mark [2] for 25 elements with $18 \leqslant Z \leqslant 96$. The Auger transition energies are of the order of initial-state energy and theoretical calculations of the transition probabilities are less sensitive to the energy values. The CK transition energies are generally considerably small and the calculated transition probabilities depend strongly on the detailed shape of the wave functions and the angular momentum coupling. Puri *et al.* [3] have tabulated the L_i subshell ($i=1,2,3$) CK (f_{ij}) and fluorescence (ω_i) yields for all the elements with $25 \leqslant Z \leqslant 96$ using the radiative transition probabilities [1] and the nonradiative transition probabilities interpolated from Ref. [2] with consideration of the cutoffs and onsets [4] of different CK transitions. Fluorescence and CK yield data have applications in areas such as fluorescence analysis, astrophysics, medical physics, and calculations of energy transport through matter under impact of the radiation.

The CK yield (f_{ij}) can be deduced from measured intensities of the L_j-subshell x rays pertaining to two cases of atomic ionization with the L_i- and L_j-subshell primary vacancies produced in widely different proportions. Jitschin [5] and Rao *et al.* [6] have reviewed different methods for measurements of the fluorescence and CK yields and listed the measurements reported after 1979. Selective photoionization, being better understood process compared to the other ionization processes, is favorably used for investigating the CK transition probabilities. Krause [7] has compiled the fluorescence and CK yields measured till 1979 for the elements with $12 \leqslant Z \leqslant 110$.

The measurements of CK yields in the atomic region $70 \leqslant Z \leqslant 83$ gains added impetus because of predicted onset of the intense L_1-$L_3M_{4,5}$ CK transitions [4] that can be manifested in the form of abrupt discontinuities in the L_1-subshell fluorescence (ω_1) and CK (f_{13} and f_{12}) yields. Werner and Jitschin [8] have measured the f_{12}, f_{23}, and f_{13} CK yields and ratios of the fluorescence yields, ω_1/ω_3 and ω_2/ω_3, for $_{72}$Hf, $_{73}$Ta, $_{74}$W, $_{77}$Ir, $_{78}$Pt, $_{79}$Au, and $_{82}$Pb elements using tunable synchrotron source. Our group has reported the L_1-L_3 CK yield (f_{13}) for $_{77}$Ir, $_{78}$Pt, and $_{83}$Bi [9], $_{82}$Pb [10], and $_{90}$Th and $_{92}$U [11] measured using the 59.54 keV γ rays and the K x rays of different elements. Some of the other recent measurements have been concluded to be inconsequent [10,12,13].

In the present investigation, the L_1-L_3 CK yield, f_{13}, for $_{70}$Yb, $_{71}$Lu, $_{74}$W, $_{75}$Re, $_{79}$Au, $_{80}$Hg, and $_{81}$Tl have been determined using measured intensities of the $L\alpha$ x rays emitted following decay of the L_i-subshell ($i=1,2,3$) primary vacancies produced in widely different proportions by the 59.54 keV γ rays ($B_{L_1} < E_{inc} < B_K$) and the Ge/Se/Rb K x rays ($B_{L_3} < E_{K\alpha} < B_{L_2}, B_{L_1/L_2} < E_{K\beta} < B_K$), where B_{K/L_i} is the K-shell/L_i-subshell binding energy of the target element. Special care has been given to incorporate corrections that may cause systematic influence on the results.

II. EXPERIMENTAL PROCEDURE

The geometrical arrangements used in the present measurements are shown in Fig. 1. These involve an annular source of ^{241}Am (300 mCi, DUPONT, U.S.) in the direct and secondary excitation modes. In the direct excitation mode, the 59.54 keV γ rays from ^{241}Am (the emission probability =35.6 per 100 decays) were used to produce primary vacancies in the L_i subshells ($i=1,2,3$) of the target element. In the

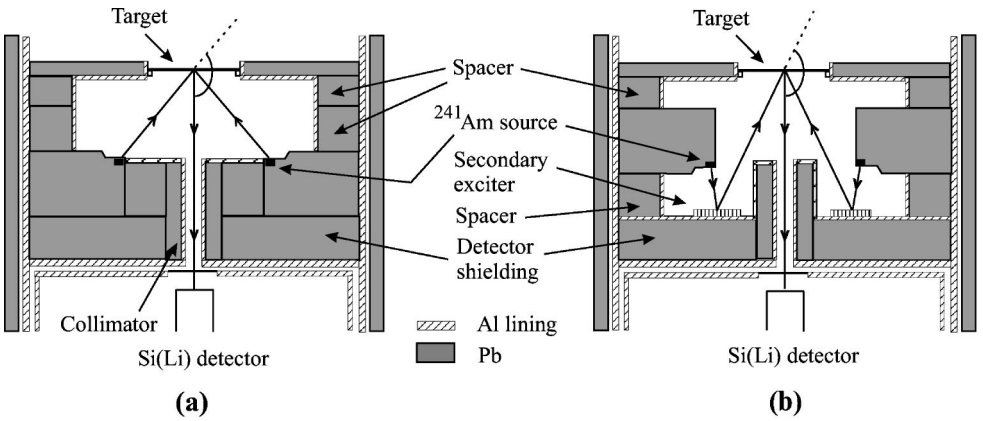

FIG. 1. Target, source, and detector geometrical arrangements in (a) direct excitation and (b) secondary excitation modes used in the present measurements.

secondary excitation mode, the 59.54 keV γ rays excited the Ge/Se/Rb $K\alpha$ and $K\beta$ x rays from the Ge/Se/RbCl secondary exciter that in turn produced the primary vacancies mainly in the L_3 subshell of the target element. The $K\beta$ x rays also produced primary vacancies either in the L_2 subshell or the L_1 and L_2 subshells of the target element. The relevant information for the different target elements and the corresponding secondary exciters is given in Table I.

Thin, spectroscopically pure foils of YbF_3 (117 $\mu g/cm^2$), LuF_3 (148 $\mu g/cm^2$), W (193 $\mu g/cm^2$), WO_3 (193 $\mu g/cm^2$), Re (21$\mu g/cm^2$), Au (108 and 287 $\mu g/cm^2$), and TlCl (184 and 225 $\mu g/cm^2$) evaporated on 6.3 μm mylar backing (Micromatter, Deer Harbor, WA, USA) were used as targets. The measurements were also performed using thick targets of Yb (82.8 mg/cm^2), Re (47.5 mg/cm^2), Au (100 mg/cm^2), and Hg(900 mg/cm^2). The Hg target was prepared by sealing Hg between the 2 μm thick mylar films. The x-ray spectra from targets were recorded with a Si(Li) detector (28.27 mm$^2\times$5.5 mm, full width at half maximum =180 eV at 5.89 keV) coupled to a PC-based multichannel analyzer (model S100, Canberra). A 6 mm diameter Pb collimator with Al lining was used with the detector. The K x-ray spectra from the Ni, Cu, Zn, GaP, Ge, GaAs, and Se targets (thickness $\sim$100 $\mu g/cm^2$) were also taken using each of the geometrical arrangements. These spectra were used to determine intensity of the exciting photons and other geometrical factors as given in the following section. Nine sets of spectra were taken with each set consisting of spectra for the above-mentioned targets using the two geometrical arrangements. The acquisition time for each spectrum was 15–25 h. The target-to-collimator and target-to-detector distances and the size of the detector collimator were kept same for all the spectra in each set. The detector viewed the same target area in both the geometrical arrangements. This minimized the possibility of error due to any nonuniformity of targets. Typical spectra taken using the Re target are shown in Fig. 2. The Lη x-ray peak for the Yb, Lu, W, and Re elements overlaps with the $L\alpha$ x-ray peak and it is well separated for the Au, Hg, and Tl elements.

III. EVALUATION PROCEDURE

The f_{13} yield is expressed in terms of the photopeak area per unit time for the $L\alpha$ x rays, $N^j_{L\alpha}(j=1,2)$, measured in case of the target excitation by the Ge/Se/Rb K x rays ($B_{L_3}<E_{K\alpha}<B_{L_2}, B_{L_1/L_2}<E_{K\beta}<B_K$) and the 59.54 keV γ rays ($B_{L_1}<E_{inc}<B_K$) as

$$f_{13}=\left(\frac{\sigma^{1\alpha}_{L_3}}{\sigma^{2'}_{L_1}}K^{1\alpha}\right)-\left(\frac{\sigma^{2'}_{L_3}}{\sigma^{2'}_{L_1}}+\frac{\sigma^{2'}_{L_2}}{\sigma^{2'}_{L_1}}f_{23}+f_{12}f_{23}\right), \qquad (1)$$

where

$$\sigma^{2'}_{L_i}=(\sigma^2_{L_i}-K^{1\beta}\sigma^{1\beta}_{L_i})$$

and

$$K^{\lambda}=\frac{N^2_{L\alpha}}{N^1_{L\alpha}}\frac{(I_oG)^{\lambda}}{(I_oG)^2}\frac{\beta^{\lambda}_{L\alpha}}{\beta^2_{L\alpha}}.$$

$\sigma^{\lambda}_{L_i}(i=1,2,3)$ are the L_i-subshell photoionization cross sections for the target element. $(I_oG)^{\lambda}$ is intensity of the exciting radiation falling on area of the target visible to the detector, and $\beta^{\lambda}_{L\alpha}$ is the self-absorption correction factor that accounts for absorption of the incident and emitted photons in the target. The superscripts $\lambda=1\alpha$ and 1β in different symbols correspond to the incident $K\alpha$ and $K\beta$ x rays, respectively, in the secondary excitation mode and the superscript $\lambda=2$ corresponds to the 59.54 keV γ rays in the direct excitation mode. The anisotropy in the emission of $L\alpha$ x rays is observed to be small ($\sim$0.1%) [15], henceforth, its effect is not considered. $\sigma^{\lambda}_{L_i}$ were interpolated from Scofield's tables [16] based on the relativistic Hartree-Fock-Slater model and are given in Table I. The f_{12} and f_{23} yields based on the RDHS model were taken from tables of Puri *et al.* [3]. These yields are of small magnitude $\sim$0.1. The use of different f_{23} values available in literature [3,7,8] does not affect the deduced f_{13} value. Although f_{12} values available in literature differ significantly, however, their use in Eq. (1) has a tiny effect on the results as it appears as product with f_{23}. The values of $\beta^{\lambda}_{L\alpha}$ have been calculated using the expression given in Ref. [17]. For the thin and thick targets used in the present measurements, $\beta^{\lambda}_{L\alpha}$ is $\sim$0.98 and $<$0.21, respectively. A value of $\beta^{\lambda}_{L\alpha}=0.21$ corresponds to 99% absorption.

Each spectrum was analyzed for the $L\alpha$ x-ray photopeak area ($N^j_{L\alpha}$) using an indigenously developed computer code

TABLE I. Characteristics of target elements and secondary exciters used in the present measurements.

Element	L_i-subshell binding energy (B_{L_i}) (keV) [14]	Secondary exciter	Energy of K x rays (keV) (Ref. [14])	$K\beta$ to $K\alpha$ x-ray intensity ratio[a] (Ref. [19])	Photoionization cross sections (barns/atom) [16] at the energy of		
					$K\alpha$ x ray	$K\beta$ x ray	59.54 keV
$_{70}$Yb	$B_{L_1}=10.489$	Ge	$E_{K\alpha}=9.876$	0.150	$\sigma_{L_1}^{1\alpha}=0$	$\sigma_{L_1}^{1\beta}=10490$	$\sigma_{L_1}^{2}=307$
	$B_{L_2}=9.978$		$E_{K\beta}=10.983$	(0.194)	$\sigma_{L_2}^{1\alpha}=0$	$\sigma_{L_2}^{1\beta}=17882$	$\sigma_{L_2}^{2}=137$
	$B_{L_3}=8.943$				$\sigma_{L_3}^{1\alpha}=38512$	$\sigma_{L_3}^{1\beta}=28930$	$\sigma_{L_3}^{2}=163$
$_{71}$Lu	$B_{L_1}=10.874$	Ge	$E_{K\alpha}=9.876$	0.150	$\sigma_{L_1}^{1\alpha}=0$	$\sigma_{L_1}^{1\beta}=10734$	$\sigma_{L_1}^{2}=321$
	$B_{L_2}=10.349$		$E_{K\beta}=10.983$	(0.194)	$\sigma_{L_2}^{1\alpha}=0$	$\sigma_{L_2}^{1\beta}=18915$	$\sigma_{L_2}^{2}=148$
	$B_{L_3}=9.245$				$\sigma_{L_3}^{1\alpha}=40564$	$\sigma_{L_3}^{1\beta}=30600$	$\sigma_{L_3}^{2}=176$
$_{74}$W	$B_{L_1}=12.098$	Se	$E_{K\alpha}=11.210$	0.163	$\sigma_{L_1}^{1\alpha}=0$	$\sigma_{L_1}^{1\beta}=9155$	$\sigma_{L_1}^{2}=365$
	$B_{L_2}=11.541$		$E_{K\beta}=12.503$	(0.212)	$\sigma_{L_2}^{1\alpha}=0$	$\sigma_{L_2}^{1\beta}=15959$	$\sigma_{L_2}^{2}=188$
	$B_{L_3}=10.204$				$\sigma_{L_3}^{1\alpha}=33541$	$\sigma_{L_3}^{1\beta}=25068$	$\sigma_{L_3}^{2}=217$
$_{75}$Re	$B_{L_1}=12.528$	Se	$E_{K\alpha}=11.210$	0.163	$\sigma_{L_1}^{1\alpha}=0$	$\sigma_{L_1}^{1\beta}=0$	$\sigma_{L_1}^{2}=385$
	$B_{L_2}=11.957$		$E_{K\beta}=12.503$	(0.212)	$\sigma_{L_2}^{1\alpha}=0$	$\sigma_{L_2}^{1\beta}=16851$	$\sigma_{L_2}^{2}=206$
	$B_{L_3}=10.534$				$\sigma_{L_3}^{1\alpha}=35242$	$\sigma_{L_3}^{1\beta}=26351$	$\sigma_{L_3}^{2}=232$
$_{79}$Au	$B_{L_1}=14.353$	Rb	$E_{K\alpha}=13.375$	0.178	$\sigma_{L_1}^{1\alpha}=0$	$\sigma_{L_1}^{1\beta}=7424$	$\sigma_{L_1}^{2}=444$
	$B_{L_2}=13.734$		$E_{K\beta}=14.980$	(0.235)	$\sigma_{L_2}^{1\alpha}=0$	$\sigma_{L_2}^{1\beta}=12826$	$\sigma_{L2}^{2}=273$
	$B_{L_3}=11.919$				$\sigma_{L_3}^{1\alpha}=26472$	$\sigma_{L_3}^{1\beta}=19565$	$\sigma_{L_3}^{2}=300$
$_{80}$Hg	$B_{L_1}=14.842$	Rb	$E_{K\alpha}=13.375$	0.178	$\sigma_{L_1}^{1\alpha}=0$	$\sigma_{L_1}^{1\beta}=7469$	$\sigma_{L_1}^{2}=461$
	$B_{L_2}=14.209$		$E_{K\beta}=14.980$	(0.235)	$\sigma_{L_2}^{1\alpha}=0$	$\sigma_{L_2}^{1\beta}=13615$	$\sigma_{L_2}^{2}=293$
	$B_{L_3}=12.283$				$\sigma_{L_3}^{1\alpha}=27750$	$\sigma_{L_3}^{1\beta}=20451$	$\sigma_{L_3}^{2}=319$
$_{81}$Tl	$B_{L_1}=15.346$	Rb	$E_{K\alpha}=13.375$	0.178	$\sigma_{L_1}^{1\alpha}=0$	$\sigma_{L_1}^{1\beta}=0$	$\sigma_{L_1}^{2}=477$
	$B_{L_2}=14.697$		$E_{K\beta}=14.980$	(0.235)	$\sigma_{L_2}^{1\alpha}=0$	$\sigma_{L_2}^{1\beta}=14160$	$\sigma_{L_2}^{2}=314$
	$B_{L_3}=12.656$				$\sigma_{L_3}^{1\alpha}=29084$	$\sigma_{L_3}^{1\beta}=21359$	$\sigma_{L_3}^{2}=339$

[a]The values within the round parentheses represent intensity ratios after correcting for absorption in the secondary exciter.

PEAKFIT [18]. The peak areas were also evaluated by subtracting the background counts, estimated by linear interpolation from above and below the photopeak, from the integral counts under the photopeak. The contribution of the overlapping $L\eta$ x-ray peak for the Yb, Lu, W, and Re elements was estimated to be ~2% using PEAKFIT, and the values agree with those evaluated using the theoretical x-ray fluorescence cross sections [19]. The ratios $(I_oG)^{\lambda}/(I_oG)^2;(\lambda=1\alpha,1\beta)$, were deduced using the measured yields of $K\alpha$ x rays of elements with $B_K<E_{K\alpha}$ selected out of the Ni, Cu, Zn, GaP, Ge, GaAs, and Se targets (thickness ~100 $\mu g/cm^2$) in the direct and secondary excitation modes and ratio of the characteristic $K\beta$ and $K\alpha$ x rays of the secondary exciter element. The procedure is detailed in our earlier paper [9].

The target $K\alpha/L\alpha$ x-ray peak areas measured in the secondary excitation mode were corrected for contribution due to ionization in the K-shell/L_i-subshells ($i=1,2,3$) by scattered photons [9]. This contribution to the $K\alpha$ x-ray peak areas is estimated to be ~3% for the thin targets, and ~4% and ~8% to the $L\alpha$ x-ray peak areas for the thin and thick Au targets, respectively. In the measurements using the thick elemental targets at 59.54 keV, the enhancement of the L_3-subshell x rays due to additional ionization by the target

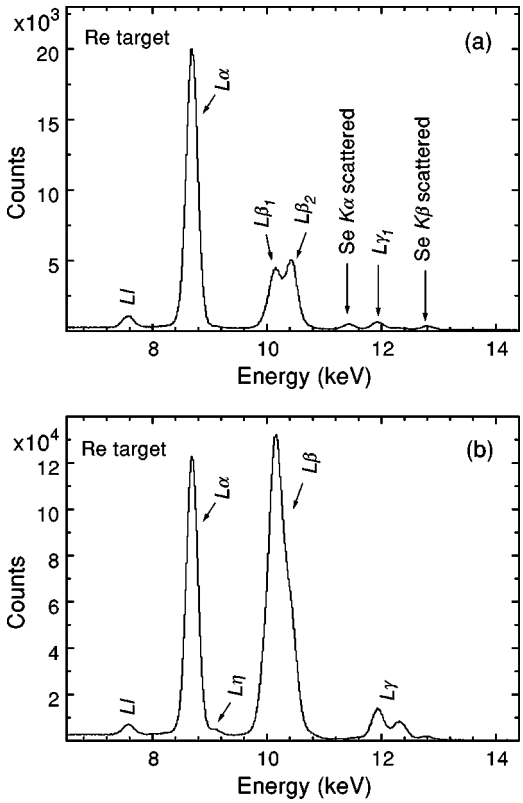

FIG. 2. Typical spectra of L x rays from the Re target excited by (a) the Se K x rays and (b) the 59.54 keV γ rays.

$L\gamma$ x rays with energies above the L_3-subshell binding energy was estimated to be ~1%. Similar measurements using thick U target have shown significant enhancement ~8%, which is mainly due to the intense $L\beta_{1,3}$ x rays having energies just above the L_3-subshell binding energy. The intensity ratios of the $L\alpha$ and $L\gamma$ x rays in the measurements done using thick and thin targets were compared for such estimation. In the measurements using the thin targets, correction due to enhancement is negligible.

IV. RESULTS AND DISCUSSION

The present measured f_{13} values for $_{70}$Yb, $_{71}$Lu, $_{74}$W, $_{75}$Re, $_{79}$Au, $_{80}$Hg, and $_{81}$Tl, deduced using different targets of an element, are found to be consistent and their average values are given in Table II. The magnitude of the expression in the second parentheses in Eq. (1) is ~50% of that in the first parentheses. The second and third terms in the second parentheses are ~12% and ~3–6%, respectively, of the first term. The error in the measured f_{13} value is estimated to be ~6% and is mainly contributed by the term within first parentheses of Eq. (1). The β factors and peak areas correspond to the same $L\alpha$ x-rays and appear as ratios in this term, therefore, most of the possible systematic errors have cancelling effects. It is noticed that the deduced f_{13} values do not change significantly even with ~5% increase or decrease in the mass-attenuation coefficients for the incident and emitted photons used to evaluate $\beta^{\lambda}_{L\alpha}$ values. It is worth mentioning that the σ_{L_1} values are substantially higher than the σ_{L_2} and

TABLE II. The f_{13} CK yields for elements with $70 \leqslant Z \leqslant 81$.

Element	f_{13} CK yield[a]		
	Present	Puri *et al.* (Ref. [3])	Krause (Ref. [7])
$_{70}$Yb	0.348 (21)	0.354	0.292
$_{71}$Lu	0.338 (21)	0.353	0.282
$_{74}$W	0.354 (24)	0.352	0.283
$_{75}$Re	0.450 (27)	0.640	0.333
$_{79}$Au	0.580 (30)	0.711	0.533
$_{80}$Hg	0.582 (30)	0.707	0.563
$_{81}$Tl	0.568 (30)	0.713	0.573

[a]Including the contribution ~1% of the intrashell L_1-L_3 radiative yield.

σ_{L_3} values for the 59.54 keV γ rays used in the present work for ionization in the L_i-subshells ($i=1,2,3$), whereas the σ_{L_2} and σ_{L_3} values dominate in case of the incident photon energies close to B_{L_1} as used in the measurements involving monochromatic synchrotron source [8], e.g., $\sigma_{L_1}:\sigma_{L_2}:\sigma_{L_3} = 100:150:225$ for W at 15 keV [16]. Hence, the present f_{13} values are expected to be more reliable.

The present measured f_{13} yields are compared with those based on the RDHS calculations [3] and the Krause's semiempirical fits [7] in Table II. The comparison is better presented in Fig. 3 by plotting these values together with the earlier measured ones [8–11] for the extended range of elements with $70 \leqslant Z \leqslant 92$. Solid line drawn in Fig. 3 indicates trend of the present and earlier measured values [8–11]. The present f_{13} values for $_{74}$W and $_{79}$Au agree within experimental error with the values 0.325(10) and 0.582(10), respectively, measured using monochromatic synchrotron source by Werner and Jitschin [8]. The f_{13} values measured by us, in general, follow the trend similar to that of the values measured by Werner and Jitschin [8]. For the elements with $70 \leqslant Z \leqslant 74$, the measured f_{13} yields agree with the RDHS values [3] and are on an average ~17% higher than the semi-

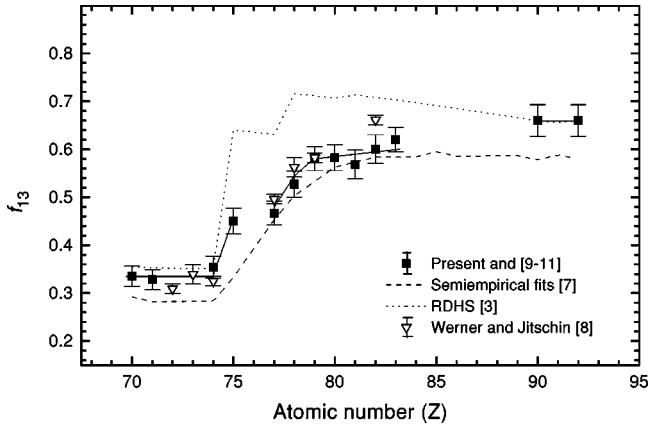

FIG. 3. The L_1-L_3 CK yield (f_{13}) as a function of atomic number. Dotted and dashed lines join the f_{13} values based on the RDHS calculations [3] and the Krause's semiempirical fits [7], respectively. Solid line indicates the trend of the present and earlier [8–11] measured values.

empirical values [7]. The measured f_{13} yield exhibits an increase from 0.354(24) for $_{74}$W to 0.450(27) for $_{75}$Re. Correspondingly, the RDHS calculations predict an increase of larger magnitude from 0.352 for $_{74}$W to 0.640 for $_{75}$Re due to onset of the L_1-L_3M_5 CK transition [4]. The present value for $_{75}$Re is ~35% higher than the semiempirical value [7]. The f_{13} values for the $_{77}$Ir, $_{78}$Pt, and $_{79}$Au elements, measured by us, exhibit an increasing trend viz. 0.467(25) [9], 0.527(27) [9], and 0.580(30), respectively, and remain nearly constant (~0.60) for the elements with $79 \leqslant Z \leqslant 83$. The present measured f_{13} values are lower than the RDHS values and closely follow the semiempirical values [7]. The RDHS based calculations predict another jump in the f_{13} yield from 0.631 for $_{77}$Ir to 0.716 for $_{78}$Pt due to onset of the L_1-L_3M_4 CK transition [4] and remain nearly constant at ~0.70 for the elements with $78 \leqslant Z \leqslant 83$. The f_{13} values measured by Werner and Jitschin [8] are also smaller in magnitude than the RDHS values and the jump in the f_{13} value at $Z=78$ is apparent. In view of the errors associated with the measurements and small magnitude of the jump, it is difficult to conclude regarding the predicted onset of the L_1-L_3M_4 CK transition [4]. For $_{90}$Th and $_{92}$U, the measured f_{13} yield [11] agree with the RDHS values. Theoretical calculations incorporating many particle interactions such as electron-electron Coulomb interactions to the available RDHS calculations [2] along with a better understanding of solid-state effects are required to apprehend the observed deviations. Further measurements in $_{75}$Re and the leftover element $_{76}$Os in different chemical environments may help to understand if some subtle effects due to exchange or relaxation effects cause a different behavior. The present and the earlier [8–11] measurements point towards the need for more refined individual-particle model calculations.

[1] J. H. Scofield, At. Data Nucl. Data Tables **14**, 121 (1974).

[2] M. H. Chen, B. Crasemann, and H. Mark, At. Data Nucl. Data Tables **24**, 13 (1979); Phys. Rev. A **24**, 177 (1981).

[3] S. Puri, D. Mehta, B. Chand, N. Singh, and P. N. Trehan, X-Ray Spectrom. **22**, 358 (1993).

[4] M. H. Chen, B. Crasemann, K. Huang, M. Aoyagu, and H. Mark, At. Data Nucl. Data Tables **19**, 97 (1977).

[5] W. Jitschin, in *X-Ray and Inner-Shell Processes*, edited by T. Carlson, O. Krause, and T. Monson, AIP Conf. Proc. 215 (AIP, New York, 1990), p. 408.

[6] P. V. Rao, Pramana, J. Phys. **50**, 669 (1998).

[7] M. O. Krause, J. Phys. Chem. Ref. Data **8**, 307 (1979).

[8] U. Werner and W. Jitschin, Phys. Rev. A **38**, 4009 (1988).

[9] Prem Singh, A. Kumar, D. Mehta, K. P. Singh, and N. Singh, Nucl. Instrum. Methods Phys. Res. B **196**, 261 (2002).

[10] A. Kumar, S. Puri, D. Mehta, B. K. Arora, and N. Singh, X-Ray Spectrom. **31**, 310 (2002).

[11] A. Kumar, S. Puri, D. Mehta, M. L. Garg, and N. Singh, X-Ray Spectrom. **31**, 103 (2002).

[12] A. Kumar, D. Mehta, and N. Singh, Phys. Rev. A **65**, 036501 (2002).

[13] A. Kumar, S. Puri, D. Mehta, and Nirmal Singh, Nucl. Instrum. Methods Phys. Res. B **183**, 227 (2001).

[14] E. Storm and H. I. Israel, Nucl. Data Tables A **7**, 565 (1970).

[15] T. Papp and J. L. Campbell, J. Phys. B **25**, 3765 (1992).

[16] J. H. Scofield, Lawrence Livermore Laboratory Report No. UCRL-51326 1973 (unpublished).

[17] D. Mehta, S. Puri, N. Singh, M. L. Garg, and P. N. Trehan, Phys. Rev. A **59**, 2723 (1999).

[18] J. Singh, R. Singh, D. Mehta, N. Singh, and P. N. Trehan, in *Proceedings of the DAE Symposium on Nuclear Physics*, edited by R. K. Choudhury and A. K. Mohanty [Nucl. Phys. B 37, 455 (1995)].

[19] S. Puri, B. Chand, D. Mehta, M. L. Garg, N. Singh, and P. N. Trehan, At. Data Nucl. Data Tables **61**, 289 (1995).